

Generation of all-fiber femtosecond vortex laser based on NPR mode-locking and mechanical LPG

Zhiming Zhang (张志明), Wei Wei (魏 薇), Liqin Tang (唐莉勤), Jie Yang (杨 洁),
Jiewei Guo (郭杰伟), Lei Ding (丁 镭), and Yigang Li (李乙钢)*

School of Physics, Nankai University, Tianjin 300071, China

*Corresponding author: liyigang@nankai.edu.cn

Received August 10, 2018; accepted September 27, 2018; posted online November 1, 2018

An all-fiber femtosecond vortex laser based on common fiber components is constructed. It can produce femtosecond orbital angular momentum modes whose time pulse width is 398 fs. The topological charge of output orbital angular momentum (OAM) modes from this laser can be adjusted among 0, +1, and -1 easily while it is also easy to convert between continuous OAM modes and pulse OAM modes.

OCIS codes: 050.4865, 140.3510, 320.7090.

doi: 10.3788/COL201816.110501.

Vortex beams having a helical phase front carry orbital angular momentum (OAM). Their analytic expression contains a phase term of $\exp(i\ell\theta)$, where ℓ is the topological charge and θ is the angular coordinate. Every photon in this beam has an OAM that equals $\ell\hbar$, where \hbar is the reduced Planck constant^[1]. Vortex beams can be applied in various areas such as optical tweezers^[2], optical trapping^[3], material processing^[4], and optical vortex knots^[5] for their donut-shape intensity and helical phase. They also provide an opportunity for applications in mode division multiplexing systems (MDMSs) because optical OAM can be another freedom that can carry information^[6], which is promising in improving the capacity of optical fiber communication systems.

Several methods producing vortex beams have been demonstrated: spatial light modulation^[7], spiral phase plate^[8], Q-plate^[9], fiber gratings^[10], cylindrical lens^[11], and optical coupler^[12]. These methods have different shortcomings such as complex configuration, low efficiency of conversion, being not easy to control, or only outputting continuous light. Wang *et al.* made femtosecond OAM laser beams based on an all fiber mode-locked laser^[13]. However, the coupler in their experimental setup cannot be changed, which means that conversion between the fundamental mode and OAM mode is impossible. Zhao *et al.* made an all fiber vortex laser that cannot output pulse vortex beam^[14]. In this Letter, an all fiber mode-locked laser with a converter producing OAM modes is constructed. It can generate femtosecond vortex beams and the topological charge of output beam is easy to adjust among 0, +1, and -1. Meanwhile, it is convenient for the transversion between continuous light and femtosecond light.

The true modes in conventional step index fiber include the fundamental mode (HE_{11}), transverse electric mode (TE), transverse magnetic mode (TM) and mixing mode ($\text{HE}_{m,n}^{\text{odd/even}}$). A vortex beam will be generated when two orthogonal mixing modes are superposed coherently with a $\pi/2$ phase difference, as shown by

$$\text{HE}_{l+1,m}^{\text{odd}} \pm i \times \text{HE}_{l+1,m}^{\text{even}} = \text{OAM}_{\pm l,m}, \quad (1)$$

where $\pm l$ is the topological charge and m is the radial index^[15].

In conventional step-index fiber, the effective index differences among many adjacent modes are less than 10^{-4} , and these modes are superposed coherently to produce the linear polarization mode. For example, TE_{01} , TM_{01} , $\text{HE}_{21}^{\text{even}}$, and $\text{HE}_{21}^{\text{odd}}$ can compose the LP_{11} mode. Similarly, the OAM mode can be generated when two orthogonal and degenerate linear polarization modes are superposed with a $\pi/2$ phase difference, as described by

$$\text{LP}_{l,m}^a \pm i \times \text{LP}_{l,m}^b = \text{OAM}_{\pm l,m}, \quad (2)$$

where $\pm l$ is the topological charge and m is the radial index^[16].

In order to produce the OAM mode in conventional step-index fiber, we need to transfer the energy from the fundamental mode in single-mode fiber (SMF) to a high-order mode in few-mode fiber. There are two methods to achieve this purpose. One method is using a coupler under the condition that phase matching is satisfied^[13,17]. The other one is applying a long-period grating (LPG) when phase matching ($\beta_{01} - \beta_{11} = 2\pi/\Lambda$) is satisfied^[14,18], where Λ is the period of grating, and β_{01} and β_{11} are propagating constants of LP_{01} and LP_{11} , respectively. In this research, the two-mode fiber (TMF) has a core diameter of 19 μm , a core refractive index of 1.449, a cladding diameter of 62.5 μm , and a cladding refractive index of 1.444. This fiber can support six true modes that can be divided into two mode groups of LP_{01} and LP_{11} . As shown in Fig. 1, dispersion curves calculated by the finite element method show the change of the effective refractive index with wavelength. According to the function $\beta = k_0 \cdot n_{\text{eff}}$, where k_0 is wave number in free space and n_{eff} is the effective index, the relationship of the grating period and the resonance wavelength can be obtained as a dotted line, as shown in Fig. 1.

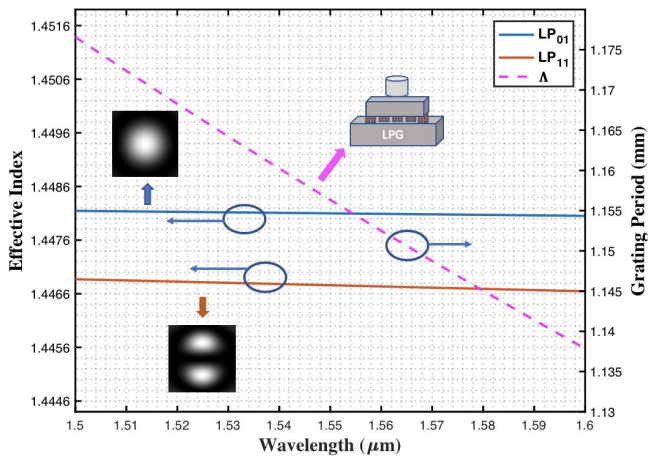


Fig. 1. Dispersion curves of LP_{01} and LP_{11} ; the relationship of the LPG period and the resonance wavelength.

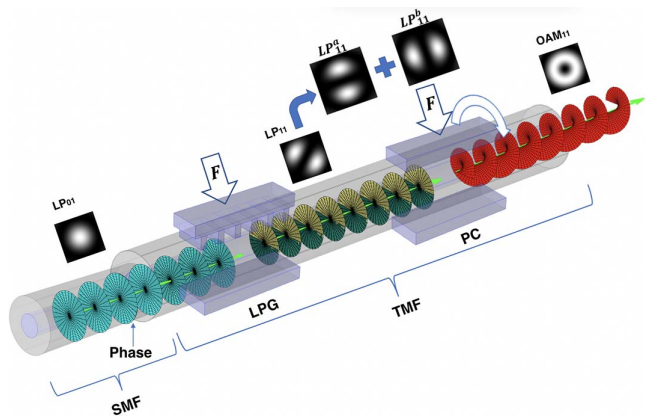


Fig. 2. Converter producing and controlling the OAM modes.

If the wavelength is 1564 nm, the grating period should be 1.15 mm to get the max efficiency of mode transversion.

The principle of mode conversion is shown in Fig. 2^[16]. The SMF and the TMF are spliced. An input LP_{01} mode from the SMF excites the LP_{01} mode in the TMF with a

low insertion loss and its wavefront is flat. Then LP_{01} is converted to LP_{11} by the LPG, which is made by stressing the TMF between mechanical gratings. LP_{11} can be decomposed into two orthogonal LP_{11}^a and LP_{11}^b at 45° relative to itself, as shown in Fig. 2. A $\pi/2$ phase difference between LP_{11}^a and LP_{11}^b can be induced by pressing TMF because the pressure changes the effective index of TMF, resulting in different phase velocities of the two modes. When the pressure applied is appropriate, the OAM mode will be created and its wavefront is helical.

First, we construct a ring nonlinear polarization rotation (NPR)^[18,19] mode-locked fiber laser to produce a femtosecond pulse laser. Then the laser passes through a converter of OAM to generate a femtosecond vortex beam. Concretely, as shown in Fig. 3, a 980 nm laser diode (LD) as a pump that has a maximum power of 390 mW inputs into the ring cavity through a wavelength division multiplexing coupler (WDM) and a highly-doped erbium fiber of 0.6 m acts as the gain medium. The polarization-dependent isolator (PD-ISO) forces unidirectional laser propagation and acts as a polarizer for NPR mode locking. Two polarization controllers (PC1 and PC2) are inserted on two sides of PD-ISO to optimize NPR mode locking. PC1, PC2, and PD-ISO act as a similar saturable absorber^[20]. A 1:9 optical coupler splits 10% of the optical power as output. The whole cavity is joined by SMF. Several optical couplers split output light to measure the power, optical spectrum, pulse trains, and so on. One path of outputs is joined to the TMF by splicing. In this path, the LPG induced by period pressure on the TMF transfers the energy from the fundamental mode to the LP_{11} mode. The grating period is adjusted to 1.15 mm and the number of periods is 30. Then the squeezer-type polarization controller is used to induce an extra $\pi/2$ phase difference between LP_{11}^a and LP_{11}^b to finally create the OAM mode. Meanwhile, in order to measure the topological charge of the OAM modes, the fundamental mode in another reference optical path is used to superpose with them coherently.

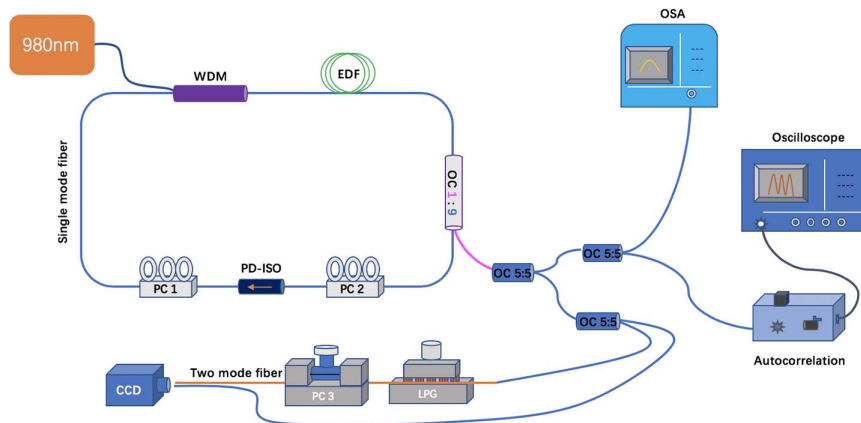


Fig. 3. Experimental setup. WDM: wavelength division multiplexing coupler; EDF: erbium-doped fiber; OC: optical coupler; PC: polarization controller; PD-ISO: polarization-dependent isolator; LPG: long period grating; CCD: charge coupled device, infrared camera; OSA: optical spectrum analyzer.

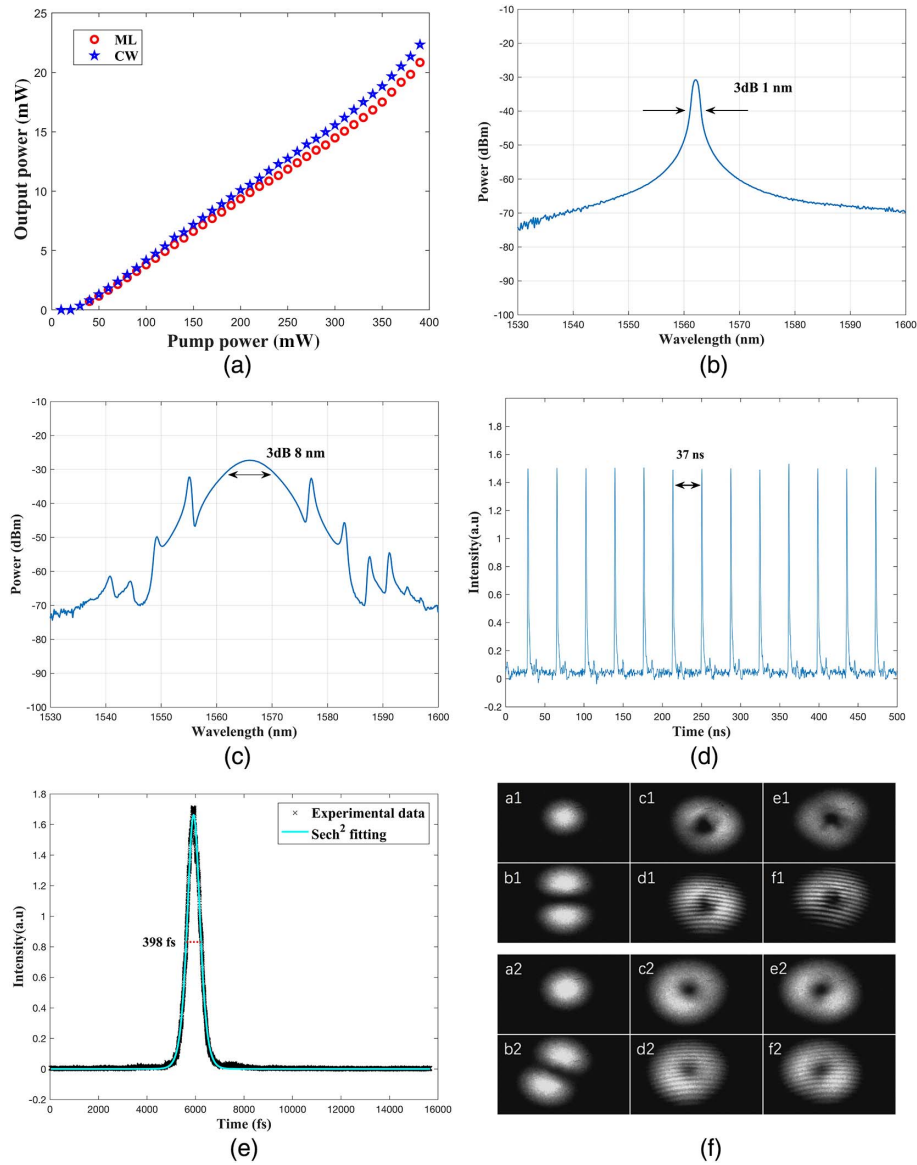


Fig. 4. (a) Relationship between the pump power and output power of the laser in the continuous state (pentagon) or mode-locked state (circle). (b) The output spectrum of the laser running in the continuous state. (c) The output spectrum of the laser running in the mode-locked state. (d) The mode-locked pulse trains recorded by the oscilloscope. (e) The pulse recorded by autocorrelation and its fitting. (f) The infrared CCD image of the near-field intensity distribution: a1–f1 are when the laser is excited in the continuous state, a2–f2 are when the laser is running in the mode-locked state. a1 and a2 are LP_{01} modes, b1 and b2 are LP_{11} modes, c1, c2, e1, and e2 are in OAM modes with topological charges of +1 and -1 , respectively; d1, d2, f1, and f2 are interference patterns of the corresponding OAM modes and reference beam.

Figure 4 shows the experimental results. As the nonlinear phase shift caused by self phase modulation and cross phase modulation is related to the intensity of light and nonlinear phase shift results in a change of polarization, adjusting PC1 and PC2 can select strong light to pass the PD-ISO to realize a similar function of a saturable absorber^[20]. Therefore, pulse light can be formed inside the cavity. It is convenient to convert the output light between the continuous and pulse states by adjusting PC1 and PC2. As shown in Fig. 4(a), the relationship of the average output power and pump power, where the pentagon line and circle line represent continuous wave (CW) output and mode-locked (ML) output, respectively,

the output power increases linearly with the pump power. The laser can work in the ML state if the pump power reaches at least 40 mW, as shown in the circle line. We define the ratio of output power to input power of the mode converter as the mode conversion efficiency. The mode conversion efficiency is measured to be about 94% in the CW state and 67% in the ML state. Because its spectrum is wider and its energy is not totally distributed on the resonance wavelength related to the period of the LPG, the conversion efficiency in the ML state is lower than in the CW state. Figure 4(b) shows optical spectrum of the continuous wave measured by OSA (YOKOGAWA AQ6370), the 3 dB bandwidth is 1 nm, and the central

wavelength is 1562 nm; Fig. 4(c) shows the optical spectrum of the pulsed light when the laser works in the mode-locked state, the 3 dB bandwidth is 8 nm, and the central wavelength is 1564 nm. The side bands feature typical soliton mode locking^[21]. We measured time pulse trains with a 200 MHz optical-electrical detector (CONQUER) and a 2.5 GHz oscilloscope (YOKOGAWA DL9140). The result shows that the laser can work in the mode-locked state stably, as shown in Fig. 4(d), the time interval of adjacent pulses is 37 ns, and the repetition rate is 27 MHz. We also measured the pulse width using an autocorrelation trace (Femtochrome Research, FR-103XL). The fitting curve according to sech^2 shows that the pulse width is 398 fs, as shown in Fig. 4(e). Finally, we recorded the intensity distribution of outputs from the TMF and their interference patterns to confirm that the setup could produce OAM modes and that the topological charge could be adjusted easily among 0, +1, and -1. As shown in Fig. 4(f), the top two rows are output patterns when the laser outputs a continuous wave while the bottom two rows are output patterns when the laser works in the mode-locked state. Only the fundamental mode in the TMF can be excited when there is no pressure on LPG and PC3, and the topological charge equals 0 as a1 and a2 shown in Fig. 4(f); then LP₁₁ mode can be obtained when a suitable pressure is applied on LPG as b1 and b2, shown in Fig. 4(f); then ± 1 order OAM modes as c1, c2, e1, and e2, shown in Fig. 4(f) can be obtained when PC3 is rotated and pressured suitably. We confirmed the topological charge of the OAM mode by the direction and the number of forks in its interference pattern. As d1 and f1, shown in Fig. 4(f), the left and right forks represent that topological charges equal +1, and -1, respectively.

In this Letter, we construct an all-fiber laser that can produce femtosecond OAM modes based on common fiber components. The topological charge of the output OAM modes from this laser can be adjusted among 0, +1, and -1 easily. Meanwhile, it can convert flexibly between continuous OAM modes and pulse OAM modes. The pulse width of the OAM modes in the time domain is 398 fs and the shorter pulse may be obtained by optimizing the dispersion in a ring cavity. After calculation, the maximum power of the single pulse is 0.74 nW and the peak power has reached 1861 W. Increasing the pump power can further increase the power of the single pulse and peak power for better application in material processing. Up to now, we have only studied one order of OAM model. If using the fiber that can support more modes to generate higher-order OAM modes, it will be of great significance for optical communication.

This work was supported by the National Natural Science Foundation of China (No. 11474170) and the Natural Science Foundation of Tianjin, China (No. 16JCYBJC16900).

References

1. L. Allen, M. Beijersbergen, R. Spreeuw, and J. Woerdman, *Phys. Rev. A* **45**, 8185 (1992).
2. M. Padgett and R. Bowman, *Nat. Photonics* **5**, 343 (2011).
3. H. Kawauchi, K. Yonezawa, Y. Kozawa, and S. Sato, *Opt. Lett.* **32**, 1839 (2007).
4. K. Toyoda, F. Takahashi, S. Takizawa, Y. Tokizane, K. Miyamoto, R. Morita, and T. Omatsu, *Phys. Rev. Lett.* **110**, 143603 (2013).
5. M. R. Dennis, R. P. King, B. Jack, K. O'Holleran, and M. J. Padgett, *Nat. Phys.* **6**, 118 (2010).
6. N. Bozinovic, Y. Yue, Y. Ren, M. Tur, P. Kristensen, H. Huang, A. E. Willner, and S. Ramachandran, *Science* **340**, 1545 (2013).
7. A. S. Ostrovsky, G. Martínezniconoff, V. Arrizón, P. Martínezvara, M. A. Olverasantamaria, and C. Rickenstorffparrao, *Opt. Express* **17**, 5257 (2009).
8. P. Schemmel, G. Pisano, and B. Maffei, *Opt. Express* **22**, 14712 (2014).
9. P. Gregg, M. Mirhosseini, A. Rubano, L. Marrucci, E. Karimi, R. W. Boyd, and S. Ramachandran, *Opt. Lett.* **40**, 1729 (2015).
10. Y. Zhao, Y. Liu, C. Zhang, L. Zhang, G. Zheng, C. Mou, J. Wen, and T. Wang, *Opt. Lett.* **42**, 4708 (2017).
11. M. W. Beijersbergen, L. Allen, H. E. L. O. van der Veen, and J. P. Woerdman, *Opt. Commun.* **96**, 123 (1993).
12. Y. Yan, J. Wang, L. Zhang, J.-Y. Yang, I. M. Fazal, N. Ahmed, B. Shamee, A. E. Willner, K. Birnbaum, and S. Dolinar, *Opt. Lett.* **36**, 4269 (2011).
13. T. Wang, F. Wang, F. Shi, F. Pang, S. Huang, T. Wang, and X. Zeng, *J. Lightwave Technol.* **35**, 2161 (2017).
14. Y. Zhao, T. Wang, C. Mou, Z. Yan, Y. Liu, and T. Wang, *IEEE Photonics Technol. Lett.* **30**, 752 (2018).
15. P. Dashti, F. Alhassen, and H. Lee, *Phys. Rev. Lett.* **96**, 043604 (2006).
16. S. Li, Q. Mo, X. Hu, C. Du, and J. Wang, *Opt. Lett.* **40**, 4376 (2015).
17. Y. Cai, J. Wang, J. Zhang, H. Wan, Z. Zhang, and L. Zhang, *Chin. Opt. Lett.* **16**, 010602 (2018).
18. H. Ahmad, S. I. Ooi, M. Z. A. Razak, S. R. Azzuhri, A. A. Jasim, K. Thambiratnam, M. F. Ismail, and M. A. Ismail, *Chin. Opt. Lett.* **15**, 051402 (2017).
19. D. Deng, L. Zhan, Z. Gu, Y. Gu, and Y. Xia, *Opt. Express* **17**, 4284 (2009).
20. D. Y. Tang, H. Zhang, L. M. Zhao, and X. Wu, *Phys. Rev. Lett.* **101**, 153904 (2008).
21. Z. Yan, H. Wang, K. Zhou, Y. Wang, C. Li, W. Zhao, and L. Zhang, *Opt. Lett.* **37**, 4522 (2012).